Article

Biosensor Enhancement Using Grooved Micromixers: Part II, Experimental Studies

Nicholas Scott Lynn Jr., Markéta Bocková, Pavel Adam, and Jiri Homola

Anal. Chem., **Just Accepted Manuscript** • DOI: 10.1021/ac504360d • Publication Date (Web): 29 Apr 2015

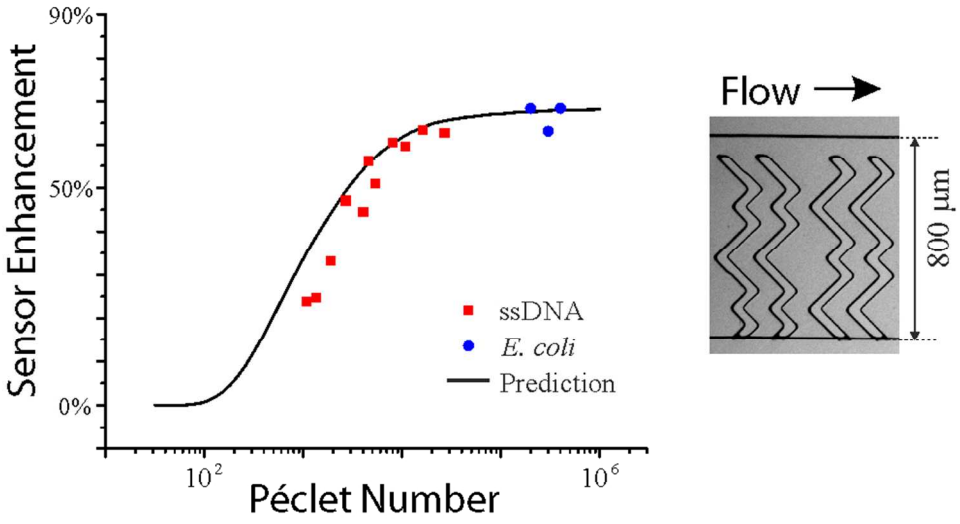

87x47mm (300 x 300 DPI)

Biosensor Enhancement Using Grooved Micromixers: Part II, Experimental Studies

N. Scott Lynn Jr., Markéta Bocková, Pavel Adam, Jiří Homola*

Institute of Photonics and Electronics, Academy of Sciences of the Czech Republic

Chaberská 57, Prague, Czech Republic

*Corresponding Author

Jiří Homola
homola@ufe.cz
Chaberská 57
Prague, Czech Republic

Abstract

In this study we examine the experimental use of the staggered herringbone mixer (SHM) for the signal enhancement of a microfluidic surface plasmon resonance imaging (SPRi) affinity-based biosensor. We define the signal enhancement (E_{mix}) as the ratio of the time-dependent slope of the sensor response of a SHM-based microfluidic channel and that of an unmixed channel; E_{mix} is directly proportional to changes in the sensor sensitivity, and inversely proportional to changes in the sensor limit of detection (LOD). Measurements were carried out for 3 SHM designs under a wide range of volumetric flow rates for two analytes: high diffusivity ssDNA and low diffusivity *E. coli* bacteria. The experimental data collected in this study was found to exhibit a good match to that predicted by the numerical methods discussed in part I of this study. We found that E_{mix} is dependent on the SHM groove geometry, the Péclet number Pe, and the overall microchannel length L; these dependencies are discussed in detail. For realistic experimental conditions, the enhancement that the SHM can provide is in the range of $1 < E_{mix} < 5$ (0% < Improvement < 400%).

Introduction

Affinity-based microfluidic biosensing technologies offer an important tool for diagnostic and analytic purposes.[1, 2] The specificity of the biorecognition element allows a biosensor to distinguish between different solutes present in a complex solution without the need for separation, and presents a major advantage with respect to traditional analytical instruments. The list of functional biorecognition elements currently in use is wide ranging, and includes antibodies, enzymes, and engineered affinity proteins;[3] cells, tissues and microorganisms;[4] and nucleic acids[5] and aptamers.[6] Likewise, the list of transduction mechanisms is also large, as there exists a variety of methods for the real-time, label-free monitoring of biomolecular interactions through optical,[7] mechanical,[8] and electrical methods.[9] Despite the wide range in biorecognition elements and transduction methods, all affinity biosensors work via the same fundamentals: a signal change is observed after an immobilized biorecognition element acts to capture the target analyte. Increasing the rate of analyte delivery to the biorecognition element will thus act to enhance the characteristic properties of the sensor, creating a higher sensitivity and a better limit of detection (LOD).

Although possessing many positive characteristics, the small size of a microfluidic sensing chamber can unfortunately contribute to effects that are detrimental to sensing. A large majority of these microfluidic biosensors have a single wall serving as the active sensing surface and are operated in a fashion such that the Reynolds number (Re) is in the laminar or Stokes regime ($\mathrm{Re} \ll 1$), with convective analyte transport occurring only in the axial direction. When the interaction between target analyte and sensor probe is mass transfer limited (occurring frequently among biosensors), an analyte boundary layer will act to reduce rates of diffusive mass transfer,[10] which can limit the detection capabilities of the sensor.

Here we turn to the use of a passive microfluidic mixing strategy to reduce the size of the analyte boundary layer, and in turn, increase the efficiency of analyte delivery to a biosensor surface. Specifically, we utilize the staggered herringbone mixer (SHM), which has previously been shown to provide an effective mixing profile on the microfluidic scale.[11] Figure 1 displays the overall design of the SHM used for sensing purposes. The sensing chamber has a height H_c, a length L, and an overall width of W_o, whereas the herringbone grooves have a symmetry width W, groove height h_g, groove width w_g, and respective inter- and intra-cycle grooves are separated axially with a pitch Λ. Although there has been an extensive amount of research regarding the optimization of the SHM for mixing purposes,[12-16] the work on the experimental use of the SHM for sensing purposes (as shown in Fig. 1)

has been limited to three studies.[17-19] Unfortunately, each of these studies involve the detection of a single analyte using a single SHM (or grooved micromixer) geometry, with each study arriving at different conclusions regarding the level of sensing enhancement the SHM can provide over that of an unmixed chamber. There remains a large gap in the literature as to how the geometry of the SHM enhances the convective and diffusive mass transfer of analyte to a sensor surface, and furthermore, how that level of enhancement depends on the operational conditions of the sensor (i.e. flow rate, analyte diffusivity).

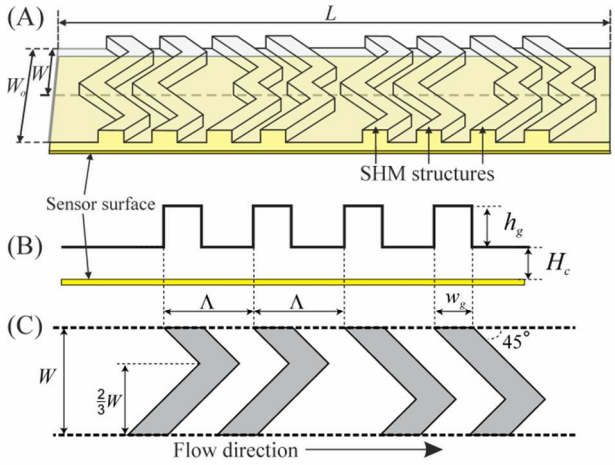

Figure 1. Design and layout of the SHM-based microfluidic sensor. (A) 3D view showing the SHM structures fabricated in a symmetric fashion in planes parallel to the axial direction. The sensor surface is colored yellow and is situated opposite the grooves. (B) side view. (C) Top view.

In part I of this study we utilized theoretical and numerical methods to characterize the ability of the SHM to enhance the level of analyte transfer to a sensor surface with respect to an unstirred rectangular channel.[20] We found that for an SHM-based channel, the analyte flux is lowest in the regions directly under the grooves and highest in the regions downstream of each groove apex. We furthermore examined how changes to the groove geometries affected the Sherwood number (Sh), a dimensionless number related to the efficiency of analyte transfer to the sensor surface. We also explored the dependence of the Sherwood number on the Péclet number (Pe). We found that a SHM-based sensor exhibits behavior similar to an unmixed system at low Pe values (with no sensing enhancement), whereas the sensing enhancement reaches an asymptotic maximum at high Pe values. These results carry significant importance for mass-transfer limited sensors: at a constant volumetric flow rate, a SHM-based sensor can give different enhancement results for the detection of two separate analytes having large differences in diffusivity.

In this study we utilize a surface plasmon resonance imaging (SPRi) biosensor to further highlight the effectiveness of a SHM-based microchannel for sensing purposes. The grooves and channel walls

are fabricated using a simple multi-layer thick film lithographic process, where sealing of the grooved microchannels to the SPRi sensor is achieved through mechanical pressure. This SHM-based SPRi biosensor is then used to characterize the sensing enhancement of three SHM geometries towards the direct detection of two model analytes having large differences in diffusivity (11-mer ssDNA and whole cell *E. coli* bacteria). In each detection experiment we control the Péclet through variation of the analyte volumetric flow rate and show that the level of sensing enhancement is dependent on Pe. These experimental results serve to verify the numerical methods developed in part I of this study,[20] which are then used to provide predictions concerning the overall range of sensing enhancements a SHM-based channel is able to provide. Although these results are specific to SPR-based sensors, the methods presented in this study are applicable to a very wide range of biosensor transduction methods, biorecognition elements, and target analytes.

Materials and Methods

Fabrication of SHM flow cells. The sidewalls and grooves of the sensing chamber consist of Su-8 photoresist (Su-8 2050, Microchem, USA), fabricated using standard multilayer lithographic techniques.[21] Lithography was performed on 35×35 mm^2 CR-39 plastic substrates (Edmund Optics, USA), which were cleaned by ozone (UVO-cleaner, Jelight Co., USA), rinsed subsequently by ethanol and DI water, and finally subjected to oxygen plasma (100 W, 30 s; Femto plasma cleaner, Diener, Germany) shortly before starting the spin coat process. The first photoresist layer was composed of either 1 or 2 independent spin coating procedures having a thickness h_g, and formed the groove layer on the top of the sensing chamber. After the soft-bake process we employed an edge bead removal step using propylene glycol monomethyl ether acetate (Microchem, USA). The photoresist film was then exposed with a broadband UV source (Intelliray 400, Uvitron, USA) through a longpass filter (L-37, Hoya Optics, USA) using a custom built mask aligner, and baked at 95°C for 20 minutes. After a second spin coating process and edge bead removal, the sample was exposed through a 2nd mask using the same custom built aligner, and subsequently hard-baked and developed, thus forming the channel sidewalls. The custom built mask aligner allowed for precision of < 50 μm in both horizontal directions, with a rotational accuracy of less than 5°. The heights of both photoresist layers were measured via a stylus profilometer (α-step 500, KLA-Tencor, USA). After the lithographic process, a mill was used to drill the fluidic inlet and outlet ports (300 μm diameter) as well as a series of alignment holes (500 μm diameter). This CR-39 chip was then aligned and sealed to a custom acrylic flow cell using a precut vinyl gasket. All fluidic inlet and outlet tubes were then attached to the acrylic

flow cell via compression ferrules (IDEX, USA). The acrylic/CR-39 chip was then sealed to the SPRi chip surface using mechanical pressure; a schematic of the arrangement is shown in Fig. 2. A calibrated peristaltic pump was used to deliver samples through each sensing channel. The entire flow cell was maintained at a constant temperature of 25 ± 0.01°C. No leaking through either the Su-8/SPRi chip or the CR-39/acrylic gasket was observed during each experiment. It should be noted that the center of each inlet port is located 250 μm from the beginning of the mixed/reference region. This inlet position provides a fully developed axial flow profile at the start of the grooved region, which allows for comparison to the numerical results in the previous portion of this study.[20]

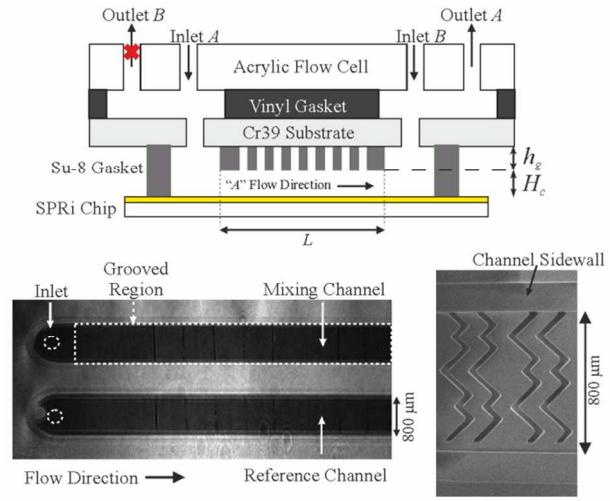

Figure 2. (top) Overall schematic of the flow cell arrangement used in this study, with outlet *B* closed through the use of an external three-way valve, the closed outlet is noted by the red mark. (bottom left) SPRi image of both a mixed and unmixed channel. For purposes of convenience, the locations of the fluidic inlets and grooved regions drawn with the dashed lines. (bottom right) SEM micrograph of a channel having $W = 200$ μm, $W_o = 800$ μm, $w_g = 50$ μm, $\Lambda = 150$ μm, $H_c = 30$ μm, and $h_g = 43$ μm.

All measurements in this study were obtained using a near-dispersionless fluidic system previously developed in our laboratory (Fig. 2).[22] The system consists of two continuous fluidic inlets (*A* and *B*) with two outlets both leading to a three-way valve, such that only one outlet port is open at any given time. By switching the state of the three-way valve (e.g. opening outlet *A* and closing outlet *B*), continuous flow from inlet B through the sensing chamber is quickly displaced by continuous flow from inlet *A* (along with a change in the flow direction). This arrangement allows for the sensor to be operated in a near dispersionless manner. The transition of change from solution *A* to solution *B*, measureable by the SPR signal along the channel length, is completed within 3 s for all of the volumetric flow rates used in this study.

SPR imaging system. In this study we utilized a self-referencing SPR imaging sensor with polarization contrast based on the Kretschmann geometry, previously developed in our laboratory.[23] Narrowband light emitted from a superluminescent diode (750 nm) is collimated, polarized, and directed at the base of a coupling prism where an SPR chip is attached via a refractive index matching fluid. The SPR chip is composed of a BK7 glass substrate, prepared for SPR imaging via the thermal evaporation of a 1 nm titanium adhesion layer followed by a 49 nm thick gold film. This gold film forms the base of the sensor surface, onto which biorecognition elements of interest are immobilized (discussed below). The light reflected from this surface passes out of the prism, through a quarter-wave plate and another polarizer, and is imaged onto a tilted CCD camera (sca780-54fm, Basler AG, Germany) via a telecentric lens (Edmund Optics). In this configuration, the spatial distribution of refractive index changes (near the sensor surface) can be correlated with the spatial distributions of intensity and the distributions of polarization changes imaged via the CCD camera. The system is referenced by off-channel areas, enabling real-time compensation for incident light intensity fluctuations.

Materials. Carboxy-terminated [HS–C_{11}–$(EG)_6$–OCH_2–COOH] and hydroxy-terminated [HS–C_{11}–$(EG)_4$–OH] alkanethiols were obtained from Prochimia (Poland). Ethanolamine hydrochloride (EA), 3-(ethyliminomethylideneamino)-N, N-dimethylpropan-1-amine (EDC), and 1-hydroxypyrrolidine-2,5-dione (NHS) were all included in Amine Coupling Kit from Biacore (Sweden). The DNA oligonucleotides Sd273 (5′-CGT GTT TGT GCC TTA TTA TTA TTA TTA TTA TTA TTA /3ThioMC3-D/-3′), TP53 (5′-GGC ACA AAC ACG CAC CTC AAA GC-3′) and d273 (5′-GC TTT GAG GTG-3′) were purchased from Integrated DNA Technologies (USA). Bovine serum albumin (BSA) was obtained from Sigma Aldrich (USA). Heat killed *E.coli* O157:H7 and its antibody were purchased from KPL (USA). All other chemicals were of analytical grade. The buffers used herein were PBS (10 mM phosphate, 2.9 mM KCl, 137 mM NaCl, pH 7.4), and PBS_{NaCl} (PBS + 500mM NaCl, pH 7.4).

Detection assays. Protocols for both mixing and reference channels were identical for both ssDNA and *E. Coli* experiments. All experiments pertaining to the direct detection of an 11-mer ssDNA were accomplished as follows. The SPR sensor surface was first functionalized via the injection of thiolated DNA probes (Sd273) at a concentration of 250 nM in PBS buffer at a volumetric flow rate Q = 5 μL/min for 30 min. This step was followed by the injection of a 20 μM blocking alkanethiol solution (HS–C_{11}–$(EG)_4$–OH) in PBS at Q = 15 μL/min for 1 hour. PBS buffer was then injected for a period of

5 min, followed by the injection of a 2 mM NaOH solution for 5 min before switching back to an injection of PBS buffer. At this point the running buffer was changed to PBS_{NaCl} and a solution of 50 nM TP53 (the middle part of the sandwich assay) was injected for 10 min at $Q = 20$ μL/min. The concentration and injection time of the TP53 was sufficient to ensure this assay step had reached equilibrium. For the final step of this assay, a 20 nM solution of d273 in PBS was injected into the sensing chamber for 10 min, where flow rates were in the range of $5 < Q < 120$ μL/min. All of the data in this study for ssDNA concerned this final (direct) detection step. This concentration was sufficiently low such that the sensor response for the first 0.5 min increased in a linear fashion with time (Fig. 3); slopes of the signal vs. time data from this region were calculated using a linear fit. We estimated the hydrodynamic radii of the 11-mer oligonucleotide using the methods of Kalwarczyk *et al*. as $r_p = 2.47$ nm, where we assumed the DNA was in the linear regime.[24] The ssDNA diffusivity was then calculated using the Stokes-Einstein equation as $D = 9.93\times10^{-11}$ m^2/s, where the viscosity of water @ 25 °C was estimated to be $\eta = 8.9\times10^{-4}$ Pa·s.

For the direct detection of *E. coli*, the SPRi chip surface was initially functionalized with a self-assembled monolayer (SAM) of mixed carboxy- and hydroxyl-terminated alkanethiols. Both the antibody against *E. coli* and the BSA blocking protein were then covalently attached to the alkanethiol SAM as described previously.[25] After immobilization of the antibodies, PBS was injected into the sensor until a stable baseline was reached. Following this, *E. coli* at a concentration of 2×10^4 CFU/mL in PBS was injected at variable flow rates for 15 minutes. Using SEM micrographs, we measured the diameter and length of the heat-killed *E. coli* to be 0.6 μm and 1.6 μm, respectively. The equivalent hydrodynamic radius and diffusivity of these bacteria was then calculated as $r_p = 760$ μm and $D = 3.2\times10^{-13}$ m^2/s.[26] It should be noted that there was no appreciable non-specific binding in both the ssDNA and *E. coli* assays.

Results and Discussion

We define the sensing enhancement as E_{mix}, the ratio of the analyte binding rate to the sensing surface between a SHM-based channel and that of an unmixed channel with equivalent H_c. The SPR sensor used in this study (along with many other label-free biosensors) provides real-time information on the rate of interaction between analyte and immobilized capture probe. It follows that the analyte binding rate is proportional to the initial time-derivative of the sensor response. For other biosensors where real-time information is not available, E_{mix} can be considered to be the ratio between the sensor response of a mixed vs. unmixed channel after a finite assay time. The convenience in this parameter is

its direct relationship to several pertinent sensor characteristics: compared to an unmixed sensor, the sensitivity of a mixed channel will be increased proportionally to E_{mix}, and the LOD will scale inversely proportional to E_{mix}.

In this study we utilize an SPRi biosensor in order to study the sensing enhancement provided by a specific groove geometry, a schematic of the sensing chamber used herein can be seen in Fig. 2. Control over the heights of the grooves and channel sidewalls (h_g and H_c) was attained via the spin coating process, whereas control over all other geometric parameters (w_g, W, W_o, L, and Λ) was attained via the design of an appropriate photomask. Each flow cell is designed to have 2-6 independent channels, where the channels are fabricated in mixing/reference channel pairs having the same effective channel height. In this arrangement, L is defined as the axial length of the 1st photoresist layer in between the fluidic inlets, as seen in Fig. 2, where for a reference channel we fabricate a uniform film of thickness h_g along this distance.

The goal of this study is to provide a quantitative examination into the enhancement that the SHM might provide to an existing sensing chamber. For this comparison, we have fabricated both reference and mixing channels with the same height H_c (for an SHM-based channel, H_c is the distance between the sensor surface and the grooves), where both channels have the same average *inlet* fluid velocity U. For purposes of comparison, we define the Péclet number as $\mathrm{Pe} = H_c U / D$, where D is the diffusivity of the target analyte. We have previously found that for a given SHM design, the ratio of the response between mixed and unmixed channels (E_{mix}) is solely dependent on Pe; therefore, the sensing enhancement for two separate analytes is expected to be the same when both detection experiments are conducted at equal Pe. We have furthermore shown that the maximum value of E_{mix} for a given SHM geometry increases as L increases.[20] Because the SPRi biosensor used here provides both spatial and temporal information, we can easily calculate E_{mix} for multiple values of L.

In order to demonstrate the use of a SHM-based channel for biosensing enhancement purposes, we examine the time- and spatially-dependent behavior of the SPRi response to a target analyte. Figure 3A shows both the mixed and unmixed sensor response to the direct detection of 11-mer ssDNA at a concentration of 20 nM. The mixer used in this experiment consisted of 4 herringbone patterns fabricated in a symmetric fashion across the width of the channel similar to that shown in Fig. 1. The data in Fig. 3A was taken as the average signal along the entire sensor length (L = 5mm). The flow rate for this detection was Q = 120 μL/min, resulting in a Péclet number of Pe = 26,900. It is clear that the sensor response of the mixed channel is higher than that of the unmixed channel. To quantify this

enhancement we calculate the maximum slope of the time-response of the sensor for each channel (shown in the dashed line), where the ratio of these slopes can be calculated as $E_{mix} = 1.63$.

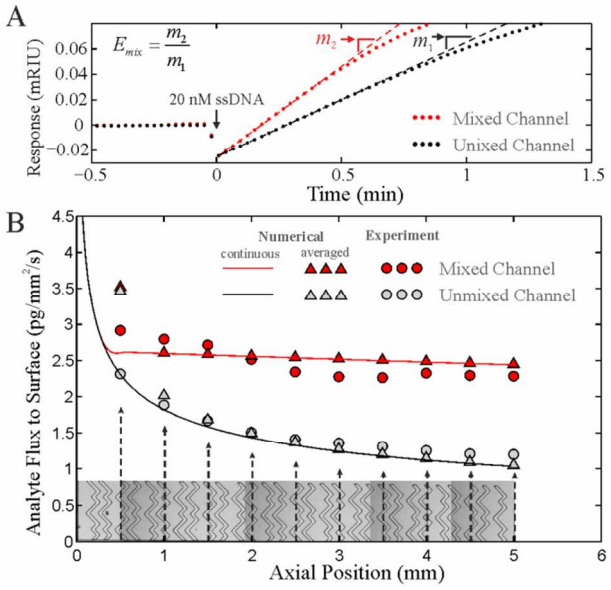

Figure 3. (A) Sensor response vs. time concerning the direct detection of 20 nM ssDNA (signal from entire channel). Both channels had dimensions $H_c = 30$ μm, $W_o = 800$ μm, and $L = 5$, with the SHM (mixed channel) having $W = 200$ μm, $h_g = 43$ μm, $w_g = 50$ μm, and $\Lambda = 150$ μm. (B) Analyte flux vs. axial position for the results shown in (A). The solid lines display continuous predicted values, whereas the triangles show averaged predicted values in 0.5 mm increments. Experimental measurements are shown in the circles.

For the sensor used here, a surface density (for biomolecules bound to the sensor surface) of 1 ng/cm^2 corresponds to a refractive index change of 0.01 mRIU;[27] therefore, we can relate the maximum slope from preselected spatial regions concerning each detection channel to calculate the analyte flux to the sensor surface. Figure 3B plots the analyte flux as a function of axial position for both the mixed and unmixed channels, where the signal from each channel was divided into segments having a length of 0.5 mm. A microscope image of the SHM-based microchannel is shown for convenience. The analyte flux from the mixed channel is higher than that of the unmixed channel at every axial position, where the difference between the two fluxes increases with increasing axial position. Also shown is the spatially dependent analyte flux predicted via our numerical methods developed in our previous study (Fig. 3).[20] These data are shown in Fig. 3 in both a continuous manner as well as a segmented (signal averaged) manner regarding the same positions as the experimental data. It should be noted that there are no adjustable parameters involved with these numerical predictions. It can be seen that there is a very good agreement between the numerical predictions and the data collected from experiment for axial positions above 1 mm. The discrepancy between numerical predictions and experiment for the $L = 0.5$ mm data can be explained by the design of the

experiment. The entire surface of the SPRi chip acts to capture analyte (Fig. 2), therefore there will be a preexisting analyte boundary layer at the beginning of the grooved region. This preexisting boundary layer will act to both (*i*) reduce the analyte flux in both mixing and reference channel with respect to the ideal (predicted) case, and (*ii*) increase the flux difference between mixed and reference channels with respect to our predictions. At larger axial positions these two effects are diminished as the axial distance of the grooved regions become much larger than the distance from the inlet to said region. Although the prediction of absolute rates of analyte flux to the surface is useful, the ratio between the mixed and unmixed flux (E_{mix}) is the parameter of interest for this study, as that ratio is expected to be independent of analyte concentration and diffusivity for a given Pe value. For the data shown in Fig. 3 we predict an enhancement of $E_{mix} = 1.65$ for the entire sensor length, very close to the observed value of 1.63. For comparison purposes, the predicted and observed enhancement for the same mixer of length $L = 2$ mm are $E_{mix} = 1.29$ and 1.48, respectively.

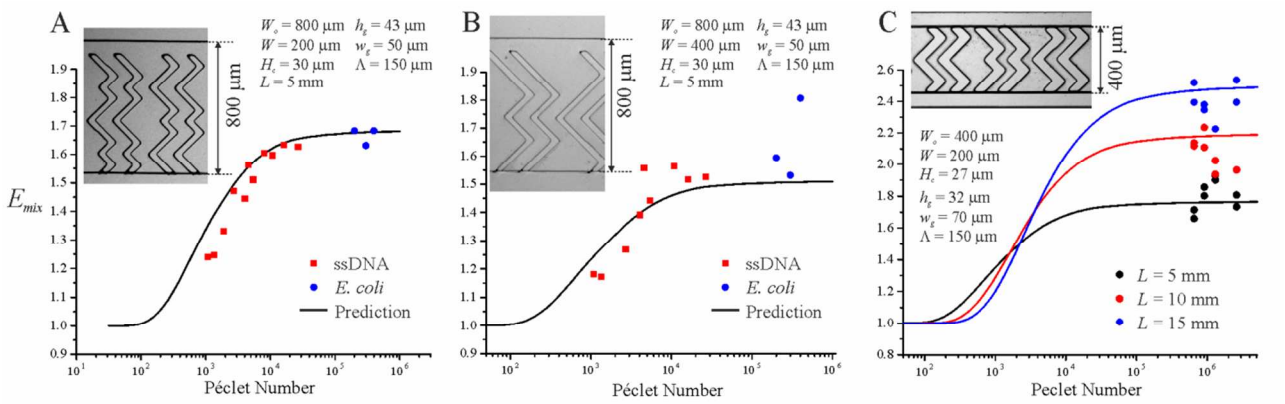

Figure 4. Sensor enhancement (E_{mix}) vs. the Péclet number for the direct detection of ssDNA and *E. coli* bacteria regarding three SHM-based groove geometries, denoted as A, B, and C. Mixer C was only used for the detection of *E. coli* bacteria. The symbols represent experimental measurements, whereas the solid lines represent predictions from part I of this study.

The data shown in Fig. 3 regard a single detection experiment for one analyte (Pe = 26,900). Part I of this study details the dependence of E_{mix} on Pe, where it was shown that E_{mix} will increase asymptotically with Pe.[20] For a given analyte and groove geometry, the Péclet number is easily modified through changes in the volumetric flow rate. For purposes of verification we repeated the experiments shown in Fig. 3 for multiple groove geometries, volumetric flow rates, and analytes. Figure 4 displays E_{mix} vs Pe for 3 different groove geometries pertaining to the direct detection of two different analytes: 11-mer ssDNA ($D = 9.93\times10^{-11}$ m^2/s), and *E. coli* bacteria ($D = 3.2\times10^{-13}$ m^2/s). These tests were performed at flow rates of $5 < Q < 120$ μL/min, where we have also included the numerical predictions for each SHM-based channel. The three mixing channels shown in Fig. 4 have

considerable variations in their geometries; however, it can be seen that the experimental measurements have a good agreement to the predicted behavior in each case. Fig. 4A and 4B regard groove geometries having differences only in the SHM symmetry width, whereas Fig. 4C regards a mixer with different groove and channel thicknesses. For a mixer length of L = 5 mm at Pe = 10^6, these mixers provide predicted enhancements of E_{mix} = 1.68 (Fig. 4A), 1.50 (4B), and 1.76 (4C). The experimental data for the detection of ssDNA highlights the importance of Pe on the ability of a SHM-based channel to provide a sensing enhancement, as there is a large variation in E_{mix} in the range of 10^2 < Pe < 10^5 for all three mixers.

Figure 4 also highlights the importance of the sensor length on the overall enhancement. The mixer shown in Fig. 4C had an overall length of L = 15 mm, where we plot the behavior of the sensor for three channel lengths (L = 5, 10, 15 mm); it can be seen that E_{mix} increases with increasing L in the high Péclet number regime. This mixer was only used towards the detection of *E. coli*, where experiments were conducted such that Pe > 10^5. In this regime the sensor enhancement is only weakly dependent on Pe, and there is very good agreement between prediction and experiment. For example, at Pe = 10^6 the mixer has a predicted enhancement of E_{mix} = 1.76, 2.18, and 2.48 for mixer lengths of L = 5, 10, and 15 mm, respectively. In comparison, for the experiments shown in Fig. 4C, the experimental measurements for E_{mix} regarding the three mixer lengths (for all Pe values) are 1.80±0.09, 2.06±0.10, and 2.40±0.1, respectively.

The data shown in Figs. 3 and 4 serve to validate and verify the numerical methods used to predict the sensing enhancement provided by the SHM,[20] and furthermore, provide some insight into the potential origin of the discrepancies observed between previous experimental studies. These methods can now be used to provide an answer to the natural question: what is the maximum enhancement that can be expected from using the SHM (or other grooved micromixers)? In part I we showed that the optimization of the SHM geometry (provided a sufficient h_g/H_c ratio) only gives small increases to E_{mix}, whereas increasing the length of such a mixer has a much stronger effect.[20] In the next section we explore the benefits and detractions of increasing L in terms of sensing performance.

The data shown in Fig. 4 were obtained in a regime such that the analyte boundary layer remained small with respect to the height of the microchannel. When an unmixed channel length increases above a critical length $L_{crit} \approx H_c\mathrm{Pe}$, the boundary layer will occupy the entire height of the channel and the sensor will approach the limit of full collection. For sensors with $L > L_{crit}$ no net enhancement can be achieved through mixing: J will be equal to the convective flux at the sensor inlet, and a wave-like

propagation of analyte flux will exist down the length of the microchannel.[28] It follows that for each SHM design there will be an optimal sensor length (constant Pe) such that E_{mix} is maximized.

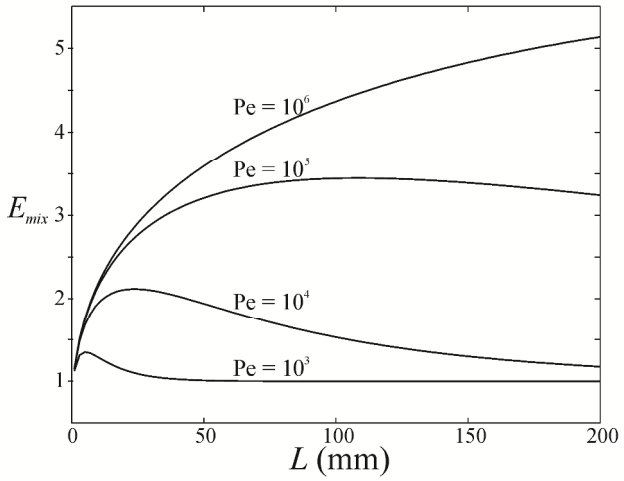

Figure 5. E_{mix} vs. the sensor length L with varying Péclet numbers. These predicted data concern a SHM having a geometry shown in Fig. 4C (W = 200 μm, H_c = 27 μm, h_g = 32 μm, w_g = 70 μm, and Λ = 150 μm).

The numerical methods developed in part I can be used to demonstrate this behavior. Figure 5 plots the sensor enhancement vs. axial length for the mixer shown in Fig. 4C at varying Péclet numbers. The behavior of these systems at low Pe values can be seen in the data for Pe = 10^3: the sensor exhibits a maximum enhancement of E_{mix} = 1.35 at a channel length of L = 5.2 mm, whereas at L_{crit} = 27 mm the sensor only exhibits an enhancement of E_{mix} = 1.07. As the Péclet number increases, there is an increase in both E_{mix} as well as the channel length that maximizes E_{mix}. The highest enhancement seen in Fig. 5 is on the edge of the parameter range, consisting of a channel of L = 200 mm at Pe = 10^6, where the mixer will provide an enhancement of E_{mix} = 5.1 (410% increase). Increases in both Pe and L can provide higher levels of sensing enhancement; however, this may lead to unrealistic experimental conditions. To date we have been unsuccessful in the search for a universal sizing guide for the design of SHM-based channels for sensing purposes (a similar guide pertaining to the use of the SHM for mixing purposes has not been published). Because of the large parameter space of the SHM-geometry, a search for the absolute maximum E_{mix} is beyond the limit of current computational techniques. Nonetheless, from the results shown in Fig. 5 it is a safe assumption that the maximum sensing enhancement for an SHM-mixed channel for reasonable experimental conditions is within the range of $E_{mix} < 10$.

The operating conditions shown in Fig. 5 are fully realizable (Pe = 10^6); for example, a sensor with an average fluid velocity of U = 1 mm/s (H_c = 27 μm), these conditions correspond to the detection of

an analyte having a diffusivity of $D = 2.7\times10^{-14}$ m^2/s, a typical value inherent to circulating tumor cells ($r_p \sim 9$ μm). Likewise, for $U = 10$ mm/s these conditions correspond to a diffusivity of $D = 2.7\times10^{-13}$ ($r_p \sim 900$ nm), values characteristic of whole-cell bacteria. The use of the SHM to detect circulating tumor cells has been previously reported by Wang *et al*., who used an 800 mm long SHM-based microchannel for the capture of EpCAM-positive cancer cell lines.[18] They reported an increase in the cell capture yield from ~60% to ~98% through the use of a SHM-based channel with respect to an unmixed channel, corresponding to a minimum enhancement of $E_{mix} = 1.63$ (although it may have been higher due to the high capture yield by the SHM-channel). Their SHM-channel had groove dimensions with a ratio of $h_g / H_c = 0.35$, which is a relatively poor ratio for SHM-based flow: all of the channels in this study had $h_g / H_c > 1.2$. From the results shown in this study, it is likely that a capture yield of ~100% could have been accomplished by Wang *et al*. using a much shorter channel provided an SHM-channel having more favorable dimensions was used. The results shown in both parts of this study can be used for the design of such an SHM.

Conclusions

The results shown in this paper serve to demonstrate the experimental use of the staggered herringbone mixer (SHM) to enhance the sensing response of an affinity-based biosensor. We have compared the time-dependent sensor response of an SHM-based channel with respect to an unmixed channel having comparable dimensions; the sensor enhancement (E_{mix}) was defined as the ratio between the slopes of said responses between the mixed and unmixed channels. We measured E_{mix} for three different SHM geometries regarding the direct detection of two analytes, 11-mer ssDNA and *E. coli* bacteria. We found that for a given SHM design, E_{mix} has a strong dependence on both the Péclet number (Pe) and the channel length (L). The experimental data collected in this study exhibit a good match to the data predicted by the numerical methods in part I of this study, this data serves as the verification and validation of those methods.[20] The enhancement values for the experimental mixers shown in this study are in the range of $1 < E_{mix} < 2.4$, where the higher end is in regards to the direct detection of *E. coli* using a mixer of length $L = 15$ mm at Pe = 10^6. This mixer is predicted to have an enhancement of $E_{mix} = 5.1$ (410% increase) for a channel of length $L = 200$ mm.

The results of this study highlight the ability of the SHM to enhance the response of a biosensor for the detection of analytes having a high Péclet number. In this regime enhancements can be seen for sensors as short as $L = 0.5$ mm (or in general the axial length of the first groove ½-cycle), where the

enhancement increases with increasing L for short channel lengths; however, one must exercise care in the sensor design, as the signal from channels having a length of $L > L_{crit}$ will exhibit no net enhancement. In this regime both the mixed and unmixed channel will be in the limit of full analyte collection and will give similar signals. The results presented in this study can be applied to a wide range of affinity-based biosensor transduction mechanisms.

Acknowledgements

This research was supported by Praemium Academiae of the Academy of Sciences of the Czech Republic and the Czech Science Foundation (contract # P205/12/G118).

References

1. A. P. F. Turner, *Chemical Society Reviews*, 2013, 42, 3184-3196.
2. S. Prakash, M. Pinti and B. Bhushan, *Philos T R Soc A*, 2012, 370, 2269-2303.
3. S. Stahl, N. Kronqvist, A. Jonsson and J. Lofblom, *J Chem Technol Biot*, 2013, 88, 25-38.
4. M. Campas, R. Carpentier and R. Rouillon, *Biotechnology advances*, 2008, 26, 370-378.
5. H. Sipova and J. Homola, *Anal Chim Acta*, 2013, 773, 9-23.
6. T. Mairal, V. C. Ozalp, P. L. Sanchez, M. Mir, I. Katakis and C. K. O'Sullivan, *Anal Bioanal Chem*, 2008, 390, 989-1007.
7. X. D. Fan and I. M. White, *Nat Photonics*, 2011, 5, 591-597.
8. J. L. Arlett, E. B. Myers and M. L. Roukes, *Nat Nanotechnol*, 2011, 6, 203-215.
9. D. Simkova and J. Labuda, *Curr Anal Chem*, 2011, 7, 2-7.
10. T. M. Squires, R. J. Messinger and S. R. Manalis, *Nature Biotechnology*, 2008, 26, 417-426.
11. A. D. Stroock, S. K. W. Dertinger, A. Ajdari, I. Mezic, H. A. Stone and G. M. Whitesides, *Science*, 2002, 295, 647-651.
12. T. G. Kang and T. H. Kwon, *J Micromech Microeng*, 2004, 14, 891-899.
13. D. G. Hassell and W. B. Zimmerman, *Chem Eng Sci*, 2006, 61, 2977-2985.
14. N. S. Lynn and D. S. Dandy, *Lab on a Chip*, 2007, 7, 580-587.
15. M. S. Williams, K. J. Longmuir and P. Yager, *Lab on a Chip*, 2008, 8, 1121-1129.
16. J. Aubin, D. F. Fletcher and C. Xuereb, *Chem Eng Sci*, 2005, 60, 2503-2516.
17. J. P. Golden, T. M. Floyd-Smith, D. R. Mott and F. S. Ligler, *Biosensors & Bioelectronics*, 2007, 22, 2763-2767.
18. S. T. Wang, K. Liu, J. A. Liu, Z. T. F. Yu, X. W. Xu, L. B. Zhao, T. Lee, E. K. Lee, J. Reiss, Y. K. Lee, L. W. K. Chung, J. T. Huang, M. Rettig, D. Seligson, K. N. Duraiswamy, C. K. F. Shen and H. R. Tseng, *Angew Chem Int Edit*, 2011, 50, 3084-3088.
19. J. O. Foley, A. Mashadi-Hossein, E. Fu, B. A. Finlayson and P. Yager, *Lab on a Chip*, 2008, 8, 557-564.
20. N. S. Lynn, 2014. Biosensor Enhancement Using Grooved Micromixers: Part I, Numerical Studies, *simultaneous submission*
21. A. Mata, A. J. Fleischman and S. Roy, *J Micromech Microeng*, 2006, 16, 276-284.
22. T. Springer, M. Piliarik and J. Homola, *Sensor Actuat B-Chem*, 2010, 145, 588-591.
23. M. Piliarik and J. Homola, *Sensor Actuat B-Chem*, 2008, 134, 353-355.

24. T. Kalwarczyk, M. Tabaka and R. Holyst, *Bioinformatics*, 2012, 28, 2971-2978.
25. K. Pimkova, M. Bockova, K. Hegnerova, J. Suttnar, J. Cermak, J. Homola and J. E. Dyr, *Anal Bioanal Chem*, 2012, 402, 381-387.
26. V. A. Bloomfield, *On-Line Biophysics Textbook: Separations and Hydrodynamics*, 2000.
27. M. Piliarik, M. Bockova and J. Homola, *Biosensors & Bioelectronics*, 2010, 26, 1656-1661.
28. T. Gervais and K. F. Jensen, *Chem Eng Sci*, 2006, 61, 1102-1121.

For Table of Contents Only